Letter

Resonant band engineering of ferroelectric tunnel junctions

Jing Su,[1] Xingwen Zheng,[1] Zheng Wen,[2] Tao Li,[3] Shijie Xie,[1] Karin M. Rabe,[4] Xiaohui Liu,[1,*] and Evgeny Y. Tsymbal[5,†]

[1]*School of Physics, State Key Laboratory of Crystal Materials, Shandong University, Ji'nan 250100, China*

[2]*College of Physics and Center for Marine Observation and Communications, Qingdao University, Qingdao 266071, China*

[3]*Center for Spintronics and Quantum Systems, State Key Laboratory for Mechanical Behavior of Materials, Department of Materials Science and Engineering, Xi'an Jiaotong University, Xi'an, Shanxi 710049, China*

[4]*Department of Physics and Astronomy, Rutgers University, Piscataway, New Jersey 08854, USA*

[5]*Department of Physics and Astronomy, University of Nebraska, Lincoln, Nebraska 68588-0299, USA*

(Received 4 February 2021; accepted 21 July 2021; published 2 August 2021)

We propose energy band engineering to enhance tunneling electroresistance (TER) in ferroelectric tunnel junctions (FTJs). We predict that an ultrathin dielectric layer with a smaller band gap, embedded into a ferroelectric barrier layer, acts as a switch controlling high- and low-conductance states of an FTJ depending on polarization orientation. Using first-principles modeling based on density functional theory, we investigate this phenomenon for a prototypical $SrRuO_3/BaTiO_3/SrRuO_3$ FTJ with a $BaSnO_3$ monolayer embedded in the $BaTiO_3$ barrier. We show that in such a composite-barrier FTJ, ferroelectric polarization of $BaTiO_3$ shifts the conduction-band minimum of the $BaSnO_3$ monolayer above or below the Fermi energy depending on polarization orientation. The resulting switching between direct and resonant tunneling leads to a TER effect with a giant ON/OFF conductance ratio. The proposed resonant band engineering of FTJs can serve as a viable tool to enhance their performance, useful for device applications.

DOI: 10.1103/PhysRevB.104.L060101

A ferroelectric tunnel junction (FTJ) is a functional electronic device with electrical resistance being controlled by ferroelectric polarization [1]. A typical FTJ is composed of two conducting electrodes separated by a nanometer-thick ferroelectric layer, which serves as a tunnel barrier. A figure of merit of an FTJ is tunneling electroresistance (TER)—a resistance change resulting from polarization reversal of the ferroelectric barrier layer [2,3]. Such polarization switching allows the control of two nonvolatile resistance states of an FTJ (low and high) which can be employed in random access memories and other electronic devices [4]. Enhancing the magnitude of TER is beneficial for device applications of FTJs.

There are several physical mechanisms responsible for the TER effect [5]. Most of them involve a modulation of the effective tunneling barrier encountered by transport electrons and driven by reversal of ferroelectric polarization [6]. Different microscopic processes control the tunneling barrier in FTJs, involving those at the interfaces, within the electrodes, as well as in the ferroelectric layer itself. An important perquisite for obtaining a large TER is asymmetry of the FTJ with respect to its electronic and atomic structure. Specifically, it has been demonstrated that a sizable TER can be obtained using dissimilar electrodes [7–13], a composite-barrier layer [14–17], and interface engineering [18–22]. Interesting physical phenomena have been predicted and demonstrated in FTJs, including ferroelectric-induced magnetic interface phase transitions [23–25], tunneling barrier metallization [26,27], defect-controlled [28–32] and bias-modulated [33,34] transport, and tunneling across an in-plane domain wall [35,36].

Despite this notable progress, further improvements in the FTJ performance are required to meet industry demands. Nowadays, due to advances in thin-film deposition techniques, growth of thin-film heterostructures can be controlled with the atomic scale precision. This allows tuning the atomic structure of FTJs within a single atomic layer to achieve the required electronic and transport properties. For example, using a layer-by-layer growth, δ doping can be realized to improve the performance of FTJs and associated electronic devices.

In this Letter we propose that the transport properties of FTJs can be significantly enhanced by inserting an ultrathin layer of a dielectric with a relatively smaller band gap in the ferroelectric barrier. Such a dielectric layer produces resonant states in the barrier energy gap which can be controlled by ferroelectric polarization. Polarization reversal shifts the conduction band of the dielectric layer up and down with respect to the Fermi level, which results in the switching of the transport regime between direct and resonant tunneling. Such a resonant band control strongly enhances an ON/OFF conductance ratio of FTJs and provides a practical tool to engineer their electronic and transport properties to meet industry requirements.

To explore this mechanism of TER, we consider a prototypical FTJ which consists of $SrRuO_3$ electrodes and a $BaTiO_3$ ferroelectric barrier with one TiO_2 atomic layer being substituted with SnO_2. The substitution of SnO_2 for TiO_2

*liuxiaohui@sdu.edu.cn

†tsymbal@unl.edu

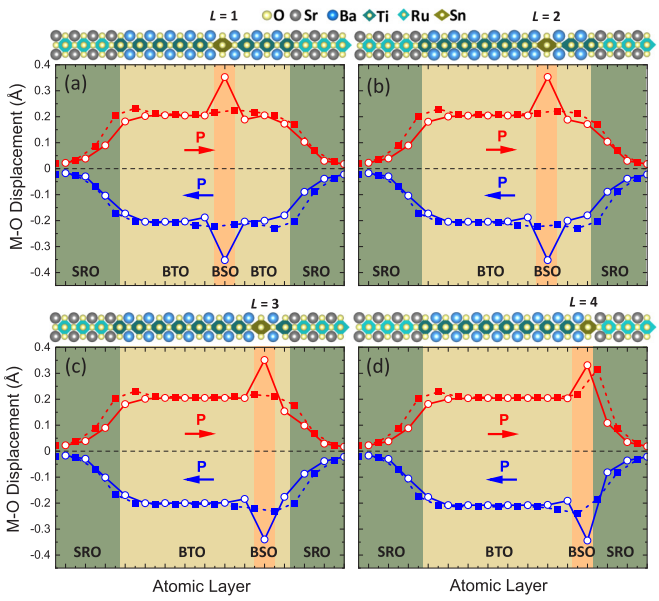

FIG. 1. Calculated relative polar displacement between cation (M) and anion (O) on each AO (squares, A = Ba or Sr) and BO_2 (circles, B = Ti, Sn, or Ru) layer across $SrRuO_3/BaTi(Sn)O_3/SrRuO_3$ supercells (top panels) with a SnO_2 monolayer placed at four different positions numbered by $L = 1$ (a), $L = 2$ (b), $L = 3$ (c), and $L = 4$ (d) as indicated by orange vertical bars. Positive (negative) values of the displacement shown in red (blue) correspond to polarization pointing to the right (left). Open (solid) symbols denote Ti-O, Sn-O, and Ru-O (Ba-O and Sr-O) displacements.

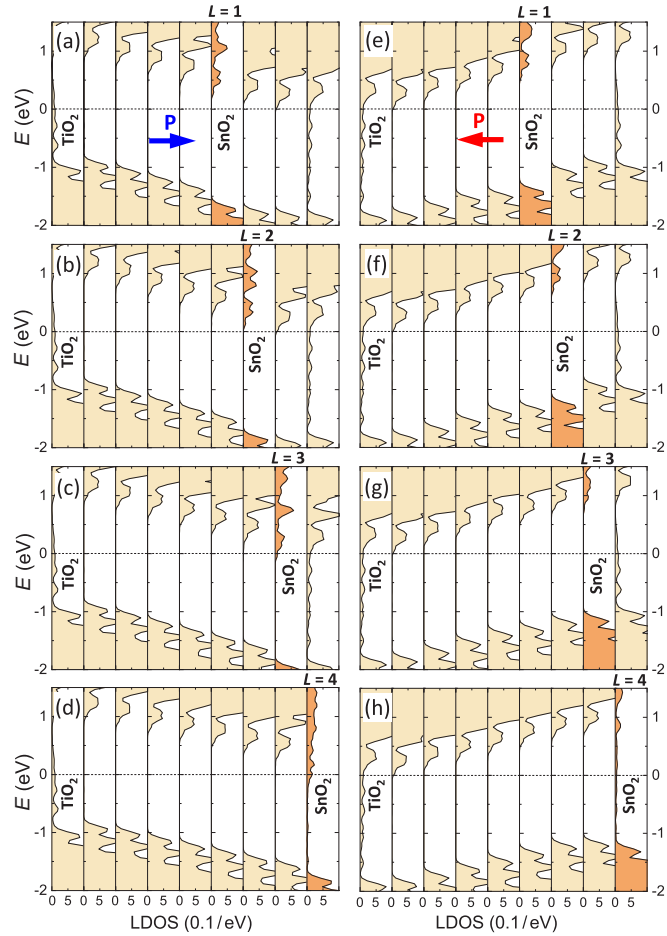

FIG. 2. Local densities of states (LDOS) as a function of energy E on each BO_2 (B = Ti, Sn) atomic layer within a composite $BaTi(Sn)O_3$ barrier for four FTJ structures with SnO_2 layer at $L = 1$ (a), (e), $L = 2$ (b), (f), $L = 3$ (c), (g), and $L = 4$ (d), (h) for polarization pointing right (a)-(d) and left (e)-(h). Horizontal dashed lines indicate the Fermi energy.

can be thought as insertion of a one-unit-cell-thick $BaSnO_3$ layer instead of that of $BaTiO_3$. $BaSnO_3$ has been predicted to exhibit a conduction-band offset with respect to $BaTiO_3$ as large as −1.13 eV [37]. In addition, $BaSnO_3$ has a similar lattice constant to $BaTiO_3$, and both $BaTiO_3$ and $BaSnO_3$ can grow epitaxially on $SrTiO_3$ [38]. Thus, if such a one-unit-cell-thick $BaSnO_3$ layer is inserted in the tunneling barrier, the conduction-band minimum (CBM) of this layer will be shifted down with respect to the CBM of $BaTiO_3$, affecting the transport mechanism. When the polarization of $BaTiO_3$ is switched between two polarization states, the CBM of $BaSnO_3$ will be pushed up and down in energy, above and below the Fermi level, so that the conduction mechanism changes from direct to resonant tunneling. This will lead to a large change in resistance of the FTJ and thus a sizable TER effect.

To confirm these expectations, we perform first-principles calculations, as described in the Supplemental Material [39–44]. In the calculations we use a supercell constructed of 8.5 unit cells of $BaTiO_3$ with one atomic layer of TiO_2 substituted by SnO_2 and 6.5 unit cells of $SrRuO_3$. The SnO_2 is placed at four different positions numbered by L, as indicated on top panels of Figs. 1(a)–1(d). To simulate coherent epitaxial growth of the structure on an $SrTiO_3$ substrate in experiment, we constrain the in-plane lattice constant of the supercell to the calculated lattice constant of cubic $SrTiO_3$, $a = 3.94$ Å. This constraint imposes an in-plane strain of about –1.5% on $BaTiO_3$ and stabilizes $BaTiO_3$ in the $P4mm$ tetragonal phase. Under this constraint, the calculated direct bands gap of $BaTiO_3$ and $BaSnO_3$ are found to be 2.5 and 1.2 eV, respectively. The smaller band gap of $BaSnO_3$ leads to the appearance of quantum-well states in the band gap of $BaTiO_3$ when Sn is substituted for Ti in a monolayer or two monolayers of $BaTiO_3$ [39].

We find that ferroelectric polarization is switchable in all FTJ structures independent of the position of the inserted SnO_2 layer. Figures 1(a)–1(d) show the respective cation-anion displacement at each AO (A = Ba or Sr) and BO_2 (B = Ti, Sn, or Ru) atomic layer in these FTJs for polarization pointing left (blue curves) and right (red curves). The Ti-O and Ba-O displacements in the barrier layer are consistent with the previous calculations for pure $BaTiO_3$ [45], reflecting a bulk-like polarization of $BaTiO_3$ independent of the position of the SnO_2 layer. It is notable that the SnO_2 layer itself behaves as a strong dipole, which is signified by a large Sn-O displacement. The presence of the Ru-O and Sr-O displacement, decaying away from the interface into the $SrRuO_3$ electrode, reflects the effect of ionic screening [46].

Figure 2 shows the calculated local density of states (LDOS) projected on TiO_2 and SnO_2 layers. It is seen that there is band bending across the barrier due to a depolarizing

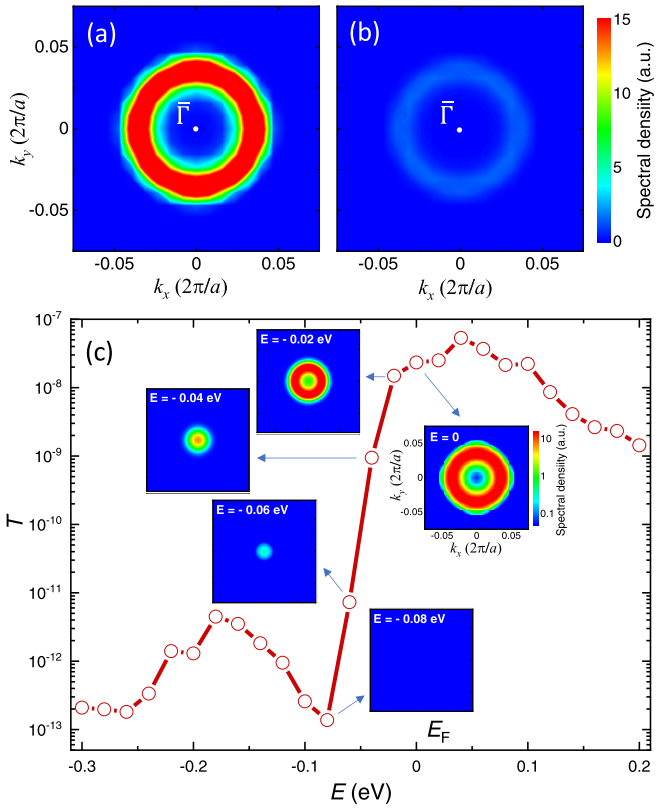

FIG. 3. Spectral density around the $\bar{\Gamma}$ point ($k_\parallel = 0$) projected onto the SnO_2 (a) and interfacial TiO_2 (b) layers at the Fermi energy for $SrRuO_3/BaTiO_3(BaSnO_3)/SrRuO_3$ FTJ with SnO_2 layer at $L = 3$ and ferroelectric polarization pointing to the right. (c) Transmission T per unit-cell area of the FTJ as a function of electron energy E. The Fermi energy E_F is at zero. Insets display spectral densities in the logarithmic scale at $E = 0$, -0.02, -0.04, -0.06, and -0.08 eV.

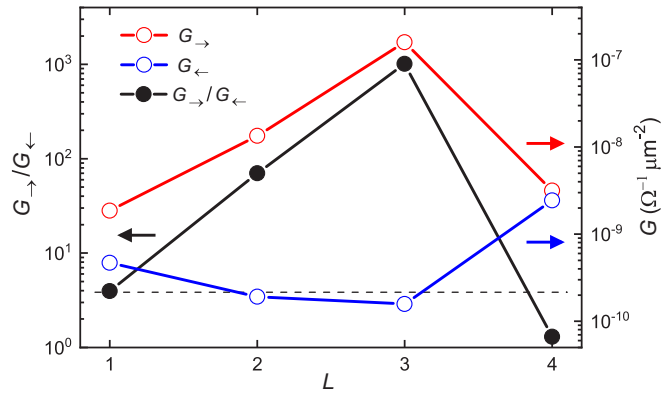

FIG. 4. Conductance G per lateral area of $SrRuO_3/BaTi(Sn)O_3/SrRuO_3$ FTJs as a function of SnO_2 layer position L in $BaTiO_3$ for polarization pointing right $G_\rightarrow$ (red dots) and left $G_\leftarrow$ (blue dots) and corresponding ON/OFF conductance ratio $G_\rightarrow/G_\leftarrow$ (black dots). The dashed line shows the junction conductance without the SnO_2 layer.

field whose direction depends on polarization orientation. For polarization pointing right [Figs. 2(a)–2(d)], the CBM on the SnO_2 layer quickly approaches the Fermi energy E_F when this layer is moved from the middle of the barrier layer ($L = 1$) to the interface ($L = 4$). When SnO_2 is in layer $L = 2$, i.e., two TiO_2 layers away from the right interface [Fig. 2(b)], the SnO_2 LDOS touches E_F, and when it is in layer $L = 3$ [Fig. 2(c)], the bottom of the SnO_2 LDOS lies about 0.2 eV below E_F. In contrast, for polarization pointing left [Figs. 2(e)–2(h)], the CBM on the SnO_2 layer lies well above the Fermi level due to the asymmetric placement of this layer closer to the right interface.

The appearance of the SnO_2 electronic states at the Fermi energy provides a resonant channel for conductance which is responsible for a large TER effect discussed below. The presence of resonant states is evident from Fig. 3(a), showing the spectral density (SD) on the SnO_2 layer around the $\bar{\Gamma}$ point ($k_\parallel = 0$) at E_F for FTJ with SnO_2 placed at $L = 3$ [corresponding to the LDOS in Fig. 2(c)]. The high SD at a ring of radius $k_\parallel \approx 0.035\frac{2\pi}{a}$ indicates the presence of a 2D free-electron-like band which is localized within the SnO_2 layer and largely composed of the Sn-2s orbital [Fig. S3(a)]. While the adjacent interfacial TiO_2 layer at the right interface is also metallized [as follows from the nonzero LDOS at E_F in Fig. 2(c)], it has a very small SD in the area around the $\bar{\Gamma}$ point where the SnO_2 SD is sizable [Fig. 3(b)]. In fact, this TiO_2 SD represents SnO_2-induced gap states, and the TiO_2-layer metallization largely results from $\boldsymbol{k}_\parallel$ lying beyond the area shown in Fig. 3(b). Therefore the interfacial TiO_2 layer provides an effective barrier for tunneling electrons with transverse wave vectors $\boldsymbol{k}_\parallel$ corresponding to the quantum-well states on SnO_2.

When the electron energy E is shifted down below E_F, the SnO_2 spectral density shrinks to a ring of a smaller radius [insets in Fig. 3(c)] and then collapses to a point [inset in Fig. 3(c) for $E = -0.06$ eV]. At $E = -0.08$ eV, there are no resonant states on SnO_2 and the transport across the FTJ is expected to occur via direct tunneling.

These expectations are confirmed by the computed transmission T as a function of energy E across the $SrRuO_3/BaTi(Sn)O_3/SrRuO_3$ FTJ with SnO_2 placed at $L = 3$ and ferroelectric polarization pointing to the right. As seen from Fig. 3(c), there is an onset of transmission at $E = -0.08$ eV so that T increases by more than five orders in magnitude with the increasing energy up to E_F. This onset is due to the transition to a resonant tunneling regime [47]. The upward trend results from the increasing number of quantum-well states contributing to transmission at a higher energy, as seen from insets in Fig. 3.

Figure 4 shows the calculated conductance per area $G = \frac{2e^2}{h}\frac{T}{A}$ (where T is transmission and A is a lateral unit-cell area of the junction) of the FTJs with different positions of the SnO_3 layer for two polarization orientations. When polarization is pointing left, the conductance $G_\leftarrow$ does not change much as the SnO_2 layer is moved from the middle of the barrier to the right interface (blue dots in Fig. 4). This is because the SnO_2 LDOS is positioned well above E_F [Figs. 2(e)–2(h)], and SnO_2 acts as a normal barrier independent of its location. In this case, the transport mechanism is controlled by direct tunneling. However, when polarization is pointing right, conductance $G_\rightarrow$ increases fast when the SnO_2 layer is moved toward the interface from $L = 1$ to $L = 3$ and then drops down

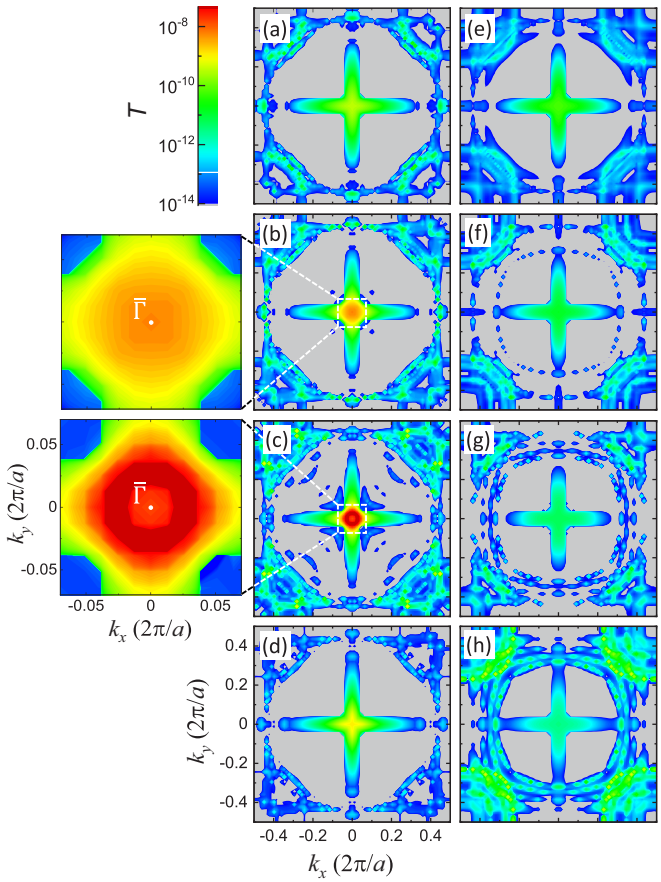

FIG. 5. $\mathbf{k}_{||}$-resolved transmission across $SrRuO_3/BaTi(Sn)O_3/SrRuO_3$ tunnel junctions with the SnO_2 layer at four different positions $L = 1$ (a), (e), $L = 2$ (b), (f), $L = 3$ (c), (g), and $L = 4$ (d), (h) for polarization pointing to the right (a)–(d) and left (e)–(h). Left panels in (b) and (c) show $T(\mathbf{k}_{||})$ zoomed in around the $\bar{\Gamma}$ point ($k_{||} = 0$).

when the SnO_2 layer is placed at the interface, $L = 4$ (red dots in Fig. 4). The increase in $G_{\rightarrow}$ is due to the band bending which pulls the SnO_2 LDOS down, reducing the tunneling barrier height. When SnO_2 is placed at $L = 3$, the SnO_2 LDOS crosses E_F, thus providing quantum-well states for resonant tunneling. Due to being separated from the $SrRuO_3$ electrode by an interfacial $BaTiO_3$ barrier layer, these resonant states strongly enhance conductance. On the contrary, when SnO_2 is placed at the interfacial layer $L = 4$, due to being in contact with conducting $SrRuO_3$, the SnO_2 effectively serves as the termination of the metal electrode. In this case the quantum well vanishes, electron transport is controlled by direct tunneling, and conductance $G_{\rightarrow}$ drops down.

To obtain more insight into the mechanism of resonant tunneling, we calculate $\mathbf{k}_{||}$-resolved transmission $T(\mathbf{k}_{||})$ across FTJs. As seen from Fig. 5, independent of the SnO_2 position and polarization orientation, $T(\mathbf{k}_{||})$ exhibits a cross feature centered at the $\bar{\Gamma}$ point in the two-dimensional (2D) Brillouin zone. This feature is intrinsic to $BaTiO_3$ whose $\mathbf{k}_{||}$-dependent evanescent states reveal the lowest decay rates along the four $\bar{\Gamma} - \bar{M}$ directions [48] and reflect direct tunneling across $BaTiO_3$. For polarization pointing left, we observe qualitatively similar $T(\mathbf{k}_{||})$ patterns controlled by the evanescent states of $BaTiO_3$ and independent of the SnO_2 location [Figs. 5(e)–5(h)]. This behavior signifies the direct mechanism of tunneling.

On the contrary, for polarization pointing right, $T(\mathbf{k}_{||})$ exhibits a "hot spot" around the $\bar{\Gamma}$ point with the transmission magnitude strongly dependent on the SnO_2 location L [Figs. 5(a)–5(d)]. The hot spot is most pronounced at $L = 3$ [Fig. 5(c)], where T is enhanced by four orders in magnitude near the $\bar{\Gamma}$ point. Zooming in on the dashed-line square of Fig. 5(c) reveals a ring feature in $T(\mathbf{k}_{||})$ around the $\bar{\Gamma}$ point [left panel in Fig. 5(c)] reminiscent of that in the spectral density [Fig. 3(a)]. This correspondence between the $T(\mathbf{k}_{||})$ and SD indicates that it is the SnO_2 quantum-well states which are responsible for the enhanced conductance $G_{\rightarrow}$ at $L = 3$ due to resonant tunneling assisted by these states.

When SnO_2 is shifted to $L = 2$, i.e., closer to the middle of the barrier, the intensity of the hot spot is reduced [Fig. 5(b)]. In this case the SnO_2 quantum-well band is shifted up in energy [Fig. 2(b)] and the resonant transmission is featured by the $T(\mathbf{k}_{||})$ distribution peaked at the $\bar{\Gamma}$ point [left panel in Fig. 5(b)]. The hot spot vanishes at $L = 1$ [Fig. 5(a)] due to the SnO_2 band being pulled above the Fermi energy [Fig. 2(a)]. When the SnO_2 layer is at the interface ($L = 4$), it becomes the termination of the metal electrode. While there is an enhanced transmission near the $\bar{\Gamma}$ point [Fig. 5(d)], it has the distinctive cross feature reflecting the evanescent states in $BaTiO_3$.

We conclude therefore that both the polarization orientation and the placement of the SnO_2 layer in the FTJ control the transport mechanism and conductance. While for polarization pointing left, the transport is governed by direct tunneling independent of the SnO_2 position, for polarization pointing right, it strongly depends on the location of the SnO_2 layer. In the latter case, when SnO_2 is placed at the second ($L = 3$) or third ($L = 2$) BO_2 layer from the interface, the conductance is strongly enhanced due to resonant tunneling. The resulting ON/OFF conductance ratio reaches a factor of 10^3 (black symbols in Fig. 4) and could be enhanced even further by proper engineering of the FTJ [49]. These density functional theory results are corroborated by a simple quantum-mechanical model of tunneling across a potential barrier which contains a quantum well [39].

In summary, we have proposed that resonant band engineering can serve as viable tool to control the mechanism of conductance and enhance the TER effect in FTJs. For a prototypical $SrRuO_3/BaTiO_3/SrRuO_3$ FTJ, we demonstrated that a single $BaSnO_3$ layer in the $BaTiO_3$ barrier could form quantum-well states supporting resonant tunneling. The effect is dependent on polarization orientation serving as a switch between resonant and direct tunneling and resulting in a giant TER effect. The proposed approach can be further elaborated to design FTJs with required performance by proper engineering of barrier, resonant band, and electrode materials and can be exploited to control spin polarization of the tunneling current. The predicted phenomenon is relevant to a ferroelectric field-effect transistor utilizing a $BaSnO_3$ channel, which is expected to exhibit a relatively high mobility [50] and can be helpful in realizing a ferroelectric resonant tunneling diode [51,52]. We hope, therefore, that our theoretical predictions will stimulate experimental studies of FTJs and related functional oxide heterostructures

with enhanced performance driven by the designed electronic bands.

The authors thank Ding-Fu Shao for valuable discussions. This work was supported by the National Natural Science Foundation of the People's Republic of China (Grants No. 11974211 and No. 11974212), the Qilu Young Scholar Program of Shandong University, and a Taishan Scholarship of Shandong Province. Z.W. acknowledges support from the Taishan Scholar Program of Shandong Province (tsqn201812045). E.Y.T. acknowledges support from NSF/EPSCoR RII Track-1: Emergent Quantum Materials and Technologies (Grant No. OIA-2044049), and from the NSF MRSEC (Grant No. DMR-1420645). Computations were performed at the Micro-Modular Data Platform of the School of Physics at Shandong University.

[1] E. Y. Tsymbal and H. Kohlstedt, Science **313**, 181 (2006).
[2] M. Y. Zhuravlev, R. F. Sabirianov, S. S. Jaswal, and E. Y. Tsymbal, Phys. Rev. Lett. **94**, 246802 (2005).
[3] H. Kohlstedt, N. A. Pertsev, J. Rodríguez Contreras, and R. Waser, Phys. Rev. B **72**, 125341 (2005).
[4] V. Garcia and M. Bibes, Nat. Commun. **5**, 4289 (2014).
[5] J. P. Velev, J. D. Burton, M. Y. Zhuravlev, and E. Y. Tsymbal, npj Comput. Mater. **2**, 16009 (2016).
[6] Z. Wen and D. Wu, Adv. Mater. **32**, 1904123 (2019).
[7] M. Y. Zhuravlev, S. Maekawa, and E. Y. Tsymbal, Phys. Rev. B **81**, 104419 (2010).
[8] D. Pantel, S. Goetze, D. Hesse, and M. Alexe, ACS Nano **5**, 6032 (2011).
[9] D. Pantel, H. Lu, S. Goetze, P. Werner, D. J. Kim, A. Gruverman, D. Hesse, and M. Alexe, Appl. Phys. Lett. **100**, 232902 (2012).
[10] Z. Wen, C. Li, D. Wu, A. Li, and N. Ming, Nat. Mater. **12**, 617 (2013).
[11] R. Soni, A. Petraru, P. Meuffels, O. Vavra, M. Ziegler, S. K. Kim, D. S. Jeong, N. A. Pertsev, and H. Kohlstedt, Nat. Commun. **5**, 5414 (2014).
[12] G. Radaelli, D. Gutiérrez, F. Sánchez, R. Bertacco, M. Stengel, and J. Fontcuberta, Adv. Mater. **27**, 2602 (2015).
[13] L. L. Tao and J. Wang, Appl. Phys. Lett. **119**, 224104 (2016).
[14] M. Y. Zhuravlev, Y. Wang, S. Maekawa, and E. Y. Tsymbal, Appl. Phys. Lett. **95**, 052902 (2009).
[15] N. M. Caffrey, T. Archer, I. Rungger, and S. Sanvito, Phys. Rev. Lett. **109**, 226803 (2012).
[16] Q. Wu, L. Shen, M. Yang, J. Zhou, J. Chen, and Y. P. Feng, Phys. Rev. B **94**, 155420 (2016).
[17] Q. Yang, L. Tao, Y. Zhang, M. Li, Z. Jiang, E. Y. Tsymbal, and V. Alexandrov, Nano Lett. **19**, 7385 (2019).
[18] A. Tsurumaki-Fukuchi, H. Yamada, and A. Sawa, Appl. Phys. Lett. **103**, 152903 (2013).
[19] H. Lu, A. Lipatov, S. Ryu, D. J. Kim, H. Lee, M. Y. Zhuravlev, C. B. Eom, E. Y. Tsymbal, A. Sinitskii, and A. Gruverman, Nat. Commun. **5**, 5518 (2014).
[20] V. S. Borisov, S. Ostanin, S. Achilles, J. Henk, and I. Mertig, Phys. Rev. B **92**, 075137 (2015).
[21] L. L. Tao and J. Wang, Appl. Phys. Lett. **108**, 062903 (2016).
[22] L. Jiang, L. L. Tao, B. S. Yang, J. Wang, and X. F. Han, Appl. Phys. Lett. **109**, 192902 (2016).
[23] J. D. Burton and E. Y. Tsymbal, Phys. Rev. B **80**, 174406 (2009).
[24] Y. W. Yin, J. D. Burton, Y. M. Kim, A. Y. Borisevich, S. J. Pennycook, S. M. Yang, T. W. Noh, A. Gruverman, X. G. Li, E. Y. Tsymbal, and Q. Li, Nat. Mater. **12**, 397 (2013).
[25] G. Radaelli, D. Gutiérrez, M. Qian, I. Fina, F. Sánchez, L. Baldrati, J. Heidler, C. Piamonteze, R. Bertacco, and J. Fontcuberta, Adv. Electron. Mater. **2**, 1600368 (2016).
[26] A. Quindeau, V. Borisov, I. Fina, S. Ostanin, E. Pippel, I. Mertig, D. Hesse, and M. Alexe, Phys. Rev. B **92**, 035130 (2015).
[27] X. Liu, J. D. Burton, and E. Y. Tsymbal, Phys. Rev. Lett. **116**, 197602 (2016).
[28] Q. H. Qin, L. Akaslompolo, N. Tuomisto, L. Yao, S. Majumdar, J. Vijayakumar, A. Casiraghi, S. Inkinen, B. Chen, A. Zugarramurdi, M. Puska, and S. V. Dijken, Adv. Mater. **28**, 6852 (2016).
[29] J. Li, N. Li, C. Ge, H. Huang, Y. Sun, P. Gao, M. He, C. Wang, G. Yang, and K. Jin, Science **16**, 368 (2019).
[30] W. Lü, C. Li, L. Zheng, J. Xiao, W. Lin, Q. Li, X. R. Wang, Z. Huang, S. Zeng, K. Han, W. Zhou, K. Zeng, J. Chen, W. C. Ariando, and T. Venkatesan, Adv. Mater. **29**, 1606165 (2017).
[31] H. Lu, D. Lee, K. Klyukin, L. L. Tao, B. Wang, H. Lee, T. R. Paudel, L.-Q. Chen, E. Y. Tsymbal, V. Alexandrov, C.-B. Eom, and A. Gruverman, Nano Lett. **18**, 491 (2018).
[32] K. Klyukin, L. L. Tao, E. Y. Tsymbal, and V. Alexandrov, Phys. Rev. Lett. **121**, 056601 (2018).
[33] D. I. Bilc, F. D. Novaes, J. Íñiguez, P. Ordejón, and P. Ghosez, ACS Nano **6**, 1473 (2012).
[34] A. Useinov, A. Kalitsov, J. Velev, and N. Kioussis, Appl. Phys. Lett. **105**, 102403 (2014).
[35] G. Sanchez-Santolino, J. Tornos, D. Hernandez-Martin, J. I. Beltran, C. Munuera, M. Cabero, A. Perez-Muñoz, J. Ricote, F. Mompean, M. Garcia-Hernandez, Z. Sefrioui, C. Leon, S. J. Pennycook, M. C. Muñoz, M. Varela, and J. Santamaria, Nat. Nanotechnol. **12**, 655 (2017).
[36] M. Li, L. L. Tao, and E. Y. Tsymbal, Phys. Rev. Lett. **123**, 266602 (2019).
[37] L. Bjaalie, B. Himmetoglu, L. Weston, A. Janotti, and C. G. Van de Walle, New J. Phys. **16**, 025005 (2014).
[38] U. Kim, C. Park, Y. M. Kim, J. Shin, and K. Char, APL Mater. **4**, 071102 (2016).
[39] See Supplemental Material at http://link.aps.org/supplemental/10.1103/PhysRevB.104.L060101 for calculation methods, band structure, and band alignment between $BaTiO_3$ and $BaSnO_3$, spectral density of resonant states as a function of energy, conductance calculations across a $SrRuO_3/BaTi(Sn)O_3/SrRuO_3$ FTJ with two $BaSnO_3$ layers inserted in the barrier, and the free-electron modeling of resonant tunneling, which includes Refs. [40–44].
[40] P. Giannozzi, S. Baroni, N. Bonini, M. Calandra, R. Car, C. Cavazzoni, D. Ceresoli, G. L. Chiarotti, M. Cococcioni, I. Dabo *et al.*, J. Phys.: Condens. Matter **21**, 395502 (2009).

[41] H. J. Choi and J. Ihm, Phys. Rev. B **59**, 2267 (1999).
[42] A. Smogunov, A. Dal Corso, and E. Tosatti, Phys. Rev. B **70**, 045417 (2004).
[43] K. D. Belashchenko, E. Y. Tsymbal, M. van Schilfgaarde, D. A. Stewart, I. I. Oleinik, and S. S. Jaswal, Phys. Rev. B **69**, 174408 (2004).
[44] Y. Ando and T. Itoh, Appl. Phys. **61**, 1497 (1987).
[45] J. P. Velev, C.-G. Duan, J. D. Burton, A. Smogunov, M. K. Niranjan, E. Tosatti, S. S. Jaswal, and E. Y. Tsymbal, Nano Lett., **9**, 427 (2009).
[46] G. Gerra, A. K. Tagantsev, N. Setter, and K. Parlinski, Phys. Rev. Lett. **96**, 107603 (2006).
[47] We note that there is a peak in transmission below the Fermi energy which is associated with the resonant state localized on the interfacial Ru atoms (see Sec. C in Supplemental Material [39]).
[48] J. P. Velev, C.-G. Duan, K. D. Belashchenko, S. S. Jaswal, and E. Y. Tsymbal, Phys. Rev. Lett. **98**, 137201 (2007).
[49] In particular, as shown in Supplemental Material [39], using two monolayers of $BaSnO_3$ in the $SrRuO_3/BaTi(Sn)O_3/SrRuO_3$ FTJ results in an ON/OFF conductance ratio which can reach a factor of 10^7.
[50] V. V. Afanas'ev, A. Stesmans, L. F. Edge, D. G. Schlom, T. Heeg, and J. Schubert, Appl. Phys. Lett. **88**, 032104 (2006).
[51] R. Du, X. Qiu, A. Li, and D. Wu, Appl. Phys. Lett. **104**, 142907 (2014).
[52] M. K. Li, N. M. Kim, S. J. Lee, J. W. Kim, and T. W. Kang, Phys. Rev. B **75**, 212106 (2007).